Research Article

Single-crystalline Ag_2Te nanorods prepared by room temperature sputtering of GeTe

Kazuki Nakaya[1] · **Toshihiro Nakaoka**[1]

Received: 23 March 2020 / Accepted: 21 August 2020 / Published online: 31 August 2020

Abstract
We report a facile, single-crystalline Ag_2Te nanorod formation based on electrochemical diffusion of Ag. The nanorods were grown non-epitaxially by sputtering deposition of GeTe on Ag_2Te nanoparticles at room temperature. For the nanorod growth, the source of the Ag supply is not deposition but the diffusion of Ag from the nanoparticles. The growth of the single-crystalline Ag_2Te nanorods required GeTe deposition onto Ag_2Te nanoparticles, in contrast to the growth of amorphous Ag_2Te nanorods caused by Te deposition onto Ag nanoparticles and the growth of other nanostructures caused by GeTe deposition on Ag nanoparticles. The GeTe deposition onto the Ag_2Te nanoparticles of an amount equivalent to a 100-nm-thick film produced nanorods of a length ranging from 3 to 5 μm and a diameter ranging from 100 to 400 nm. We propose a model for the nanorod growth based on solid-state electrochemical reaction between GeTe and movable Ag ions, inducing nanoscale phase separation and precipitation of amorphous Ge. We suggest that the nanorod structure with a crystalline Ag_2Te core and an amorphous Ge shell is useful for thermoelectric applications.

Keywords GeTe · Ag_2Te · Nanorod · Nanowire · Nanoparticle · Electrochemical reaction · RF magnetron sputtering

1 Introduction

The electrochemical reaction of Ag in amorphous chalcogenides of solid electrolytes has been investigated intensively because of the fundamental interests in anomalous diffusion [1], modified phase change characteristics [2, 3], and optical properties [4–6] and also because of the potential device applications [7] such as RAM memories, sensors, and batteries. For example, the operation of conductive bridge RAM (CBRAM) devices [8, 9] is based on the formation of conductive filaments via the electrochemical reaction of Ag ions. We have directly observed the formation of conductive filaments in GeTe [10], which is a typical phase change material used in phase change RAM [11, 12], radio frequency switches [13, 14], CBRAM [15, 16], and thermoelectric devices [17–19].

Such an electrochemical reaction has also been used for crystal growth in silver chalcogenides [20, 21]. Bulk single crystals of Ag_2S and Ag_2Se were grown based on the electrochemical diffusion of Ag that determined the growth rate [22, 23]. Amorphous [24] or polycrystalline [25] Ag_2Te films were obtained by electrochemical interdiffusion between deposited Te and an Ag film at room temperature. Not only bulk crystals, but also nanostructures can be produced by the electrochemical reaction [26–28]. Ag_2S whiskers or nanowires were grown electrochemically from an Ag plate, placed in a sulfur vapor environment, and kept at a fixed temperature for more than an hour. In this paper, we report on the electrochemical formation of single-crystalline Ag_2Te nanorods by magnetron sputtering at room temperature with a normal deposition rate of ~ 1 A/s. Formation of a single-crystalline Ag_2Te nanorod requires deposition of "GeTe" onto "Ag_2Te" nanoparticles. This contrasts with the formation of amorphous Ag_2Te nanorods that requires deposition of "Te" onto "Ag" nanoparticles [29]. Electrochemical phase separation of Ge as

✉ Toshihiro Nakaoka, nakaoka@sophia.ac.jp | [1]Faculty of Science and Technology, Sophia University, Tokyo 102-8554, Japan.

well as the Ag_2Te seeds is essential for the crystallization. To the best of our knowledge, this is the first report on electrochemical formation of the single-crystalline one-dimensional structures produced by dry or vacuum-deposition processes such as evaporation, sputtering, and chemical vapor deposition, which are compatible with semiconductor technology.

Ag_2Te is a narrow gap semiconductor [30, 31] that has various attractive properties, including near-infrared light emission [32, 33], large magnetoresistance [34, 35], structural phase transition [36], topological insulating behaviors [37, 38], and a high thermoelectric figure of merit ZT [39–41]. One-dimensional structures including nanofibers, nanorods, or nanowire can modify the properties. An enhancement of the ZT in one-dimensional Ag_2Te has been reported [42, 43] and was attributed to modified phonon scattering [44, 45] and electronic contribution [46]. Such one-dimensional structures of Ag_2Te have also been applied to flexible thermoelectric [47, 48] and electronic [49] devices. The flexible devices require lower temperatures for growth or processing than the decomposition temperatures of the flexible substrates, which are typically between 100 and 300 °C [50].

The one-dimensional Ag_2Te nanostructures have been fabricated mostly via chemical solution synthetic routes [42–51] such as electrochemical transformation in an electrochemical solution from Ag nanofibers to Ag_2Te nanotubes [52], possibly because chemical solution synthetic routes were potentially mass-producible and low cost. On the other hand, dry or vacuum-deposition processes such as evaporation, sputtering, and chemical vapor deposition have been little used despite their advantages for avoiding contamination and their high purity. Reported single-crystalline Ag_2Te nanowires grown by a dry or vacuum process without the help of an electrochemical reaction have generally required high growth temperatures around 1000 °C [53, 54] and a relatively long reaction time of more than several tens of minutes in a furnace. No facile deposition methods around room temperature have yet been presented.

2 Materials and methods

The Ag_2Te nanoparticles used as the seeds for the nanorod growth were prepared by thermal annealing of an Ag film in Te vapor. A 10-nm-thick Ag film was formed by RF magnetron sputtering with an Ag target (99.99% purity) on a 300-nm-thick SiO_2 layer thermally oxidized on a (100) Si substrate. The Ag film was annealed at 500 °C for three hours in Te vapor that was evaporated from Te powder placed upstream to the Ag film and was carried by Ar gas at a flow rate of 10 sccm. The fabricated seed nanoparticles had an average diameter of about 100 nm and a density of about $5 \times 10^9/cm^2$ (Fig. 1a). The structure was identified as monoclinic Ag_2Te crystal slightly including cubic Ag on the basis of the X-ray diffraction (XRD) pattern (Fig. 1b). The XRD measurement was performed in an asymmetric, 2θ scan mode with a small incident angle fixed at 0.5°, using a Rigaku Smart Lab diffractometer with a Cu source at an acceleration voltage of 45 kV and a current of 200 mA.

Nanorods were spontaneously grown by depositing GeTe on the slightly Ag-rich $Ag_{2+\delta}Te$ nanoparticles by RF magnetron sputtering without intentional heating. A temperature increase of less than 50 °C during the deposition was confirmed by a label-type temperature indicator. The GeTe was deposited at a rate of 1.2 Å/s using a GeTe target (99.99% purity), with a plasma discharge power of 50 W, under an argon flow of 30 sccm, and at a pressure of 0.7 kPa. We emphasize here that the nanorods were grown without an Ag supply from the deposition. The only possible source of Ag was the diffusion from the nanoparticles of $Ag_{2+\delta}Te$. Because GeTe deposition lowers the concentration of Ag near the surface, the Ag ions are continuously driven by the concentration gradient from the nanoparticles toward the surfaces. The diffusion constant of monoclinic Ag_2Te was reported to be around 10^{-4} cm^2 s^{-1} at 110 °C [55]. The diffusion constant was three orders of magnitude lower than that of the high-temperature cubic phase, which is a well-known super ionic semiconductor [56, 57], but the diffusion was still significant in microscale. Extrapolation assuming the Arrhenius law suggests ~ 10 μm^2 s^{-1} at RT. Thus, the ion diffusion rate was faster than the deposition rate of 1.2 Å/s.

The structure and the composition of a nanorod were identified by transmission electron microscopy (TEM), electron diffraction measurement, and energy-dispersive

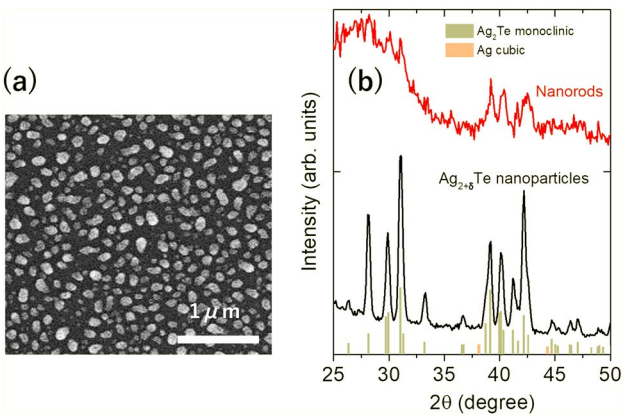

Fig. 1 **a** SEM image of the $Ag_{2+\delta}Te$ nanoparticles. **b** XRD patterns of the nanoparticles and those after GeTe deposition producing nanorods. Standard crystalline patterns of monoclinic Ag_2Te (# 00-034-0142) and cubic Ag (# 01-071-4613) are also shown

X-ray (EDX) spectroscopy using a JEOL JEM-ARM200F with an accelerating voltage of 200 kV.

3 Results and discussion

The GeTe deposition onto the $Ag_{2+\delta}Te$ nanoparticles of an amount equivalent to a 100-nm-thick film spontaneously produced nanorods of a length ranging from 3 to 5 μm and a diameter ranging from 100 to 400 nm (Fig. 2a). The nanorods grew at a density of about $8 \times 10^7/cm^2$ with no preferred growth orientation. A typical cross-sectional TEM image of a nanorod is shown in Fig. 2b. Electron diffraction patterns were measured at the core (A–D) and the cover layer (E) of the nanorod (Fig. 2c). All the diffraction patterns measured along the nanorod core (A–D) were successfully indexed as monoclinic Ag_2Te (JCPDS No. 00-034-0142) and were the same in geometric arrangements and the orientation: Some difference in spot contrast was attributed to an extrinsic bending caused during the specimen fabrication for the TEM measurement. This demonstrates that the nanorod core consists of a single-crystalline Ag_2Te. The growth of crystalline Ag_2Te was also confirmed by the XRD measurement on the nanorod sample (Fig. 1b). Sharp peaks of monoclinic Ag_2Te were superimposed on a broad spectrum of Ag-diffused amorphous GeTe arising from the other regions than the nanorods. The different relative intensity of the Ag_2Te peaks between the nanorod sample and the seed sample suggests the nanorod growth having a different orientation tendency with the seed nanoparticles.

The position of the diffraction spot of (4–2–2) shows that the nanorod grew along [4–2–2] or [2–1–1], and the positions of the spots of (200) and (1–2–2) represent that two facet planes on the top are (100) and (– 122), respectively. As shown in Fig. 3a, the facet of (100) was capped

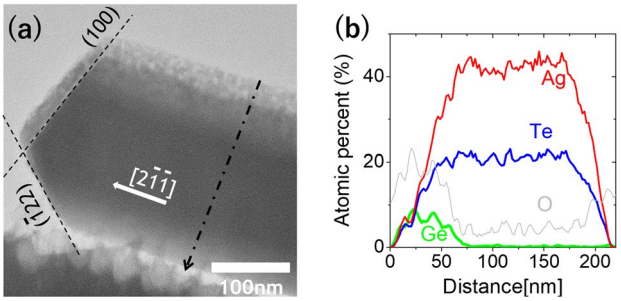

Fig. 3 **a** TEM image enlarged near the tip of the nanorod of Fig. 2b. **b** Line profiles of EDX spectrometry along the line indicated by a dashed-and-dotted arrow in (**a**)

with a cover layer about 10 nm thick, while that of the (– 122) plane was not capped. EDX mapping in a radial direction shows that the cover layer consists of Ge_xO_{1-x} (Fig. 3b). The electron diffraction of the cover layer (E) showed a halo pattern, characteristic of an amorphous structure in contrast to the diffraction of the core (A-D) that showed the spot patterns from the Ag_2Te crystal. The Ge_xO_{1-x} most likely resulted from extrinsic oxidation of Ge after exposure to the ambient air because the base vacuum for the deposition was less than 5.0×10^{-5} Pa. In other words, the cover layer intrinsically consisted of amorphous Ge. The EDX mapping also shows twice as much Ag as Te in the nanorod core, which confirms that the core consisted of Ag_2Te (Fig. 3b).

GeTe was deposited mainly as free atoms. The free Te atoms deposited onto an Ag-rich part of the $Ag_{2+\delta}Te$ nanoparticle react with Ag to form Ag_2Te. However, direct Te deposition at similar deposition conditions onto $Ag_{2+\delta}Te$ nanoparticles did not produce nanorods (Fig. 4). Because the free energy of formation of Ag–Te is much lower than that of Ge–Te, Ge is phase-separated and is precipitated. The cover layer formation of amorphous Ge in our Ag_2Te

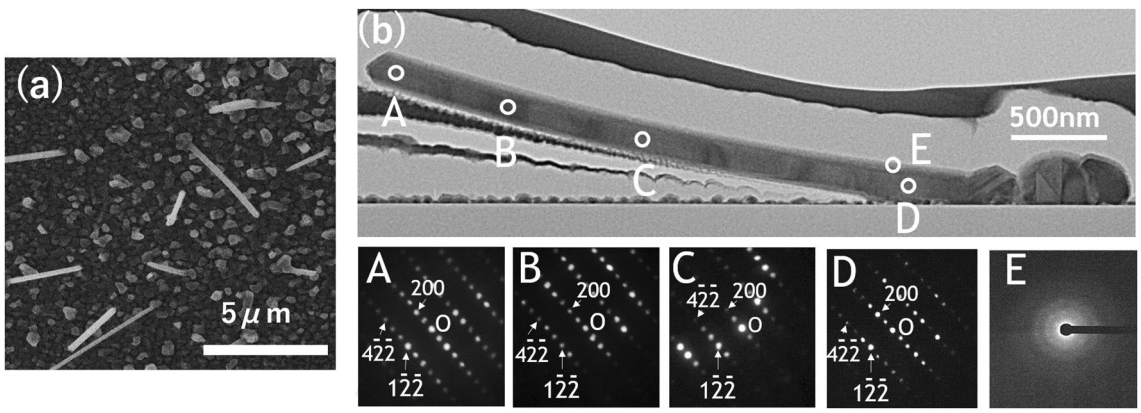

Fig. 2 **a** SEM image of nanorods. **b** TEM image of a nanorod and electron diffraction patterns taken with an incident electron beam along [0–11], measured at the points A–D indicated by white circles. The diffraction patterns at A–D are indexed as monoclinic Ag_2Te

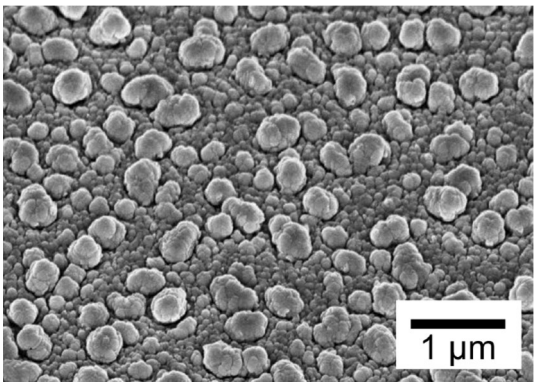

Fig. 4 SEM image of $Ag_{2+\delta}Te$ nanoparticles after Te deposition onto them. Te deposition at 1.2 Å/s of an amount equivalent to a 100-nm-thick film produced no nanorods

nanorods is attributed to the amorphous Ge precipitation that occurs as a result of the nanoscale phase separation to form Ag_2Te. The nanoscale phase separation resulting in precipitated amorphous Ge regions was also observed in the case of the GeTe deposition onto Ag nanoparticles [58]. We suggest that the supply of Ge that leads to the precipitation is required to grow the reacted Ag_2Te into the 3–5-μm-long single-crystalline Ag_2Te nanorods. The importance of the Ge precipitation for the Ag_2Te crystalline nanorod formation is supported by the observations that Te deposition onto Ag nanoparticles at the deposition condition produced *amorphous* Ag_2Te nanorods [29]. Thus, forming single-crystalline nanorods requires a supply of Ag via diffusion, a supply of Ge, and the $Ag_{2+\delta}Te$ nanoparticles as the seed.

The nanorod grew along [2–1–1] and had two facets of (100) and (– 122) on the top. The facet of (100) was capped with an about 10-nm-thick amorphous Ge layer, while that of the (– 122) plane was not capped. The nanorod growth along [2–1–1] is attributed to the characteristic of monoclinic Ag chalcogenides that forms dendritic whiskers for the restricted supply of silver ions via diffusion and the competitive growth along [100] and [1, 2]. The direction [100] is one of the favorable growth directions in the Ag–Te topotactic reaction when depositing Te onto Ag film [59]. Kasugabe demonstrated that monoclinic Ag_2S whisker grew along several peculiar branching directions such as [310] and [410] after the saturation of the growth along the principal growth direction of [100] due to the restricted supply [26]. In the case of our Ag_2Te nanorod growth, we suggest that the growth along [100] was slowed down due to the formation of the amorphous Ge regions. The growth along [100] was not stopped because the amorphous Ge region still allows for the diffusion to supply Ag. Assuming three times faster growth along [100] than [1, 2] results in the growth along [2–1–1]. The Ge layer formed on the (100) growth plane can decrease the growth rate along [100]. We suggest that the slowed growth along [100] induced additional growth along [1, 2]. The growth along [1, 2] did not suffer from Ge precipitation because the (1–2–2) plane was face-down and was shadowed from the GeTe deposition.

The interface between the bottom of the nanorod and the nanoparticle was studied by TEM and electron diffraction measurements (Fig. 5a–c). At point F, which is a point on the interface, the diffraction patterns were observed in two series. One was the same as the patterns of the nanorod core found at points A–D in Fig. 3b, and the other was the same as that of the nanoparticle found at point G. The two patterns were of the monoclinic Ag_2Te in different orientations. The electron beam incident direction corresponded to the [0–11] direction for the nanorod and the [– 1–11] direction for the nanoparticle. The interface consisted of the (2–1–1) plane of the nanorod and the (3–21) plane of the nanoparticle. The different atomic arrangements of the two planes indicated that the nanorod growth was not epitaxial. One key feature of the nanorod–nanoparticle orientation was that the (1–1–1) plane of the nanorod, which consisted of only Ag atoms, is in parallel to the (1–10) plane of the nanoparticle, which also consisted of only Ag atoms (Fig. 5c, d). We suggest that the parallel Ag-only plane pair with movable Ag atoms forms a locally Ag-rich region that facilitates Ag diffusion and eases the non-epitaxial growth to form Ag_2Te nuclei. The important role of the parallel Ag-only planes on the nanorod growth explains the low nanorod yield of about 2%. In other words, the low yield can be improved if the orientation of the seed nanoparticles is controlled.

In light of all these considerations, we propose a model for nanorod growth: (1) A solid-state interdiffusion reaction occurs between GeTe and Ag when GeTe is deposited on an $Ag_{2+\delta}Te$ seed nanoparticle with locally Ag-rich regions, such as Ag-only layers. (2) The reaction induces a nanoscale phase separation of Ge to form Ag_2Te and to precipitate Ge. (3) Further deposition of GeTe and subsequent interdiffusion partly reduces the Ag concentration in the formed Ag_2Te region, which serves to retain the Ag diffusion from the seed nanoparticle toward the top, and repeats the solid-state reaction between GeTe and Ag to form Ag_2Te. (4) When the size of the Ag_2Te region becomes greater than the critical nucleus size, the embryo starts to grow, and movability of Ag atoms on Ag-only planes of monoclinic Ag_2Te eases the formation of the nucleus and the non-epitaxial growth. The indirect supply of Ag allows for an appropriate rate of one-dimensional crystal growth.

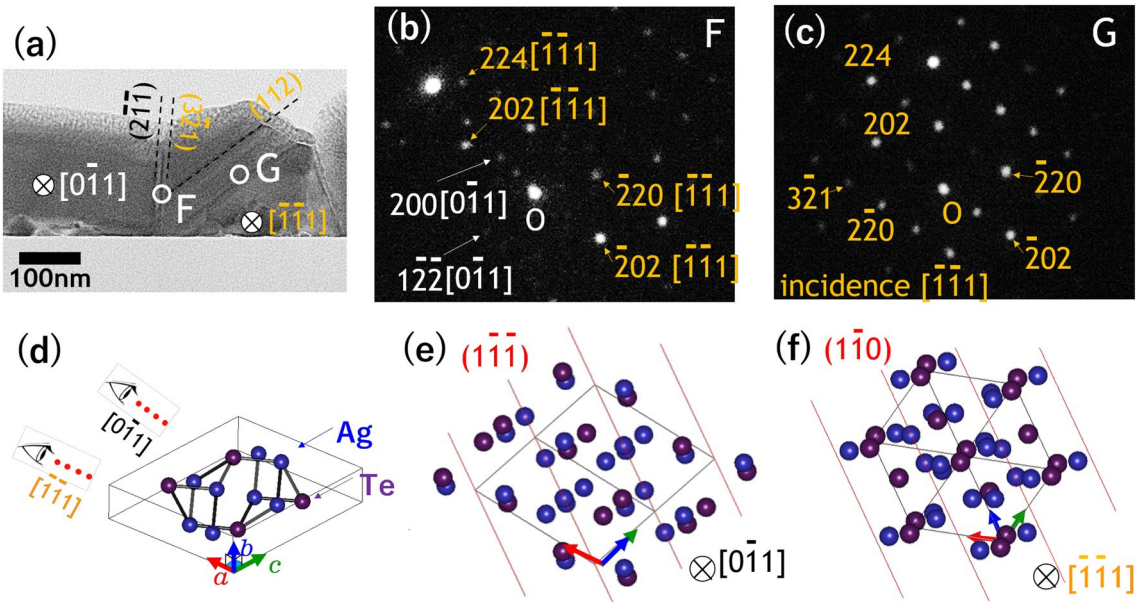

Fig. 5 **a** Cross-sectional TEM image enlarged near the bottom of the nanorod. **b** Electron diffraction pattern, measured at point F, and **c** at point G, whose positions are indicated by the circles in (**a**). Both diffraction patterns at F and G are indexed as monoclinic Ag_2Te. **d** Atomic arrangement in a unit cell of the monoclinic Ag_2Te displayed in a bird's eye view. **e** Cross-sectional atomic arrangement, perpendicular to the electron beam direction, around a unit cell of the nanorod and **f** that of the nanoparticle, oriented like those shown in the TEM image (**a**). The atomic arrangements were obtained using the ReciPro software package [60]

4 Conclusions

We have demonstrated a facile, room temperature, dry-deposition-based growth of single-crystalline monoclinic Ag_2Te nanorods with a thin amorphous cover layer of Ge. The single-crystalline Ag_2Te nanorods were grown by GeTe deposition onto $Ag_{2+\delta}Te$ nanoparticles, in contrast to the amorphous Ag_2Te nanorods grown by Te deposition onto Ag nanoparticles and the broccoli-like nanostructures formed by GeTe deposition onto Ag nanoparticles. We propose a model for non-epitaxial single-crystalline nanorod growth on the basis of the electrochemical diffusion of Ag and reaction with GeTe, involving nanoscale phase separation.

The nanorod structure with a crystalline Ag_2Te core and an amorphous Ge shell has two advantages for thermoelectric applications. One arises from the crystalline core/amorphous shell structure. The crystalline core/amorphous shell structure modifies the vibrational modes to decrease the thermal conductivity [61, 62]. The other arises from the combination of the materials of Ag_2Te and Ge. The bandgap of Ag_2Te [63] is lower than that of Ge and thus confines electronic carriers in the core, while the thermal conductivity of Ag_2Te [40] is comparable to or smaller than Ge [64] and thus induces phonon transport in the shell, resulting in decoupled electronic and phononic transport [65].

Acknowledgements This work was supported in part by MEXT KAKENHI Grant Numbers 18H01480 and by specially promoted academic research from Sophia University.

Compliance with ethical standards

Conflict of interest The authors declare that they have no conflict of interest.

References

1. Kolobov A, Elliott S (1991) Photodoping of amorphous chalcogenides by metals. Adv Phys 40:625–684. https://doi.org/10.1080/00018739100101532
2. Song K-H, Kim S-W, Seo J-H, Lee H-Y (2009) Influence of the additive Ag for crystallization of amorphous Ge–Sb–Te thin films. Thin Solid Films 517:3958–3962. https://doi.org/10.1016/j.tsf.2009.01.128
3. Han JH, Jeong K-S, Ahn M et al (2017) Modulation of phase change characteristics in Ag-incorporated $Ge_2Sb_2Te_5$ owing to changes in structural distortion and bond strength. J Mater Chem C 5:3973–3982. https://doi.org/10.1039/c6tc05412a
4. Singh P, Sharma P, Sharma V, Thakur A (2017) Linear and nonlinear optical properties of Ag-doped $Ge_2Sb_2Te_5$ thin films estimated by single transmission spectra. Semicond Sci Technol 32:045015. https://doi.org/10.1088/1361-6641/aa5ee0
5. Singh P, Singh A, Sharma J et al (2018) Reduction of rocksalt phase in Ag-doped $Ge_2Sb_2Te_5$: a potential material for reversible near-infrared window. Phys Rev Appl 10:054070. https://doi.org/10.1103/physrevapplied.10.054070
6. Singh P, Kaur R, Sharma P, Sharma V, Thakur A (2018) Effect of visible light on the structural and optical properties of

$(Ge_2Sb_2Te_5)_{100-x}$ Ag_x (x = 0, 1 and 3) thin films. J Mater Sci Mater Electron 29:1042–1047. https://doi.org/10.1007/s10854-017-8004-1
7. Frumar M, Wagner T (2003) Ag doped chalcogenide glasses and their applications. Curr Opin Solid State Mater Sci 7:117–126. https://doi.org/10.1016/S1359-0286(03)00044-5
8. Ielmini D, Waser R (eds) (2015) Resistive switching: from fundamentals of nanoionic redox processes to memristive device applications. Wiley, Weinheim
9. Hasegawa T, Terabe K, Tsuruoka T, Aono M (2012) Atomic switch: atom/ion movement controlled devices for beyond Von-Neumann computers. Adv Mat 24:252–267. https://doi.org/10.1002/adma.201102597
10. Imanishi Y, Kida S, Nakaoka T (2016) Direct observation of Ag filament growth and unconventional SET-RESET operation in GeTe amorphous films. AIP Adv 6:075003. https://doi.org/10.1063/1.4958633
11. Bruns G, Merkelbach P, Schlockermann C et al (2009) Nanosecond switching in GeTe phase change memory cells. Appl Phys Lett 95:043108. https://doi.org/10.1063/1.3191670
12. Ielmini D, Lacaita AL (2011) Phase change materials in non-volatile storage. Mater Today 14:600–607. https://doi.org/10.1016/S1369-7021(11)70301-7
13. Wang M, Lin F, Rais-Zadeh M (2016) Need a change? Try GeTe: A reconfigurable filter using germanium telluride phase change RF switches. IEEE Microwave Mag 17:70–79. https://doi.org/10.1109/MMM.2016.2608699
14. King MR, El-Hinnawy N, Borodulin P et al (2018) Connecting post-pulsing electrical and microstructural features in GeTe-based inline phase change switches. J Appl Phys 124(19):195103
15. Jin MM, Cheng L, Li Y et al (2018) Reconfigurable logic in nanosecond Cu/GeTe/TiN filamentary memristors for energy-efficient in-memory computing. Nanotechnology 29:385203. https://doi.org/10.1088/1361-6528/aacf84
16. Goux L, Radhakrishnan J, Belmonte A et al (2019) Key material parameters driving CBRAM device performances. Faraday Discuss 213:67. https://doi.org/10.1039/C8FD00115D
17. Bayikadi KS, Sankar R, We CT et al (2019) Enhanced thermoelectric performance of GeTe through in situ microdomain and Ge-vacancy control. J Mater Chem A 7:15181–15189. https://doi.org/10.1039/C9TA03503F
18. Xing T, Song Q, Qiu P et al (2019) Superior performance and high service stability for GeTe-based thermoelectric compounds. Nat Sci Rev 6:944–954. https://doi.org/10.1093/nsr/nwz052
19. Warzoha RJ, Donovan BF, Vu NT, Champlain JG, Mack S, Ruppalt LB (2019) Nanoscale thermal transport in amorphous and crystalline GeTe thin-films. Appl Phys Lett 115:023104. https://doi.org/10.1063/1.5098334
20. Bruce PG (2003) Solid state electrochemistry. Cambridge University Press, Cambridge
21. Kharton VV (2011) Solid state electrochemistry. Wiley, Weinheim
22. Ohachi T, Yamamoto T, Taniguchi I (1974) The single crystal growth of α-Ag_2S and α-Ag_2Se controlled by the diffusion of silver atoms at the solid/vapour interface. J Cryst Growth 24:576–580. https://doi.org/10.1016/0022-0248(74)90382-0
23. Ohachi T, Taniguchi I (1977) Growth of α-Ag_2S and α-Ag_2Se single crystals in a solid/vapour system. J Cryst Growth 40:109–117. https://doi.org/10.1016/0022-0248(77)90035-5
24. Hauser JJ (1982) Electrical and structural properties of Ag-X diffusion couples (X = Te, Se, S, and I). J Appl Phys 53:3634–3638. https://doi.org/10.1063/1.331145
25. Mohanty BC, Kasiviswanathan S (2006) Transmission electron microscopy and Rutherford backscattering spectrometry studies of Ag_2Te films formed from Ag–Te thin film couples. Cryst Res Tech 41:59–63. https://doi.org/10.1002/crat.200410530
26. Kasukabe S (1983) Growth mechanism and growth form of β-Ag_2S whiskers. J Cryst Growth 65:384–390. https://doi.org/10.1016/0022-0248(83)90078-7
27. Okabe T, Nakagawa M (1979) Growth of α-Ag_2S whiskers in a VLS system. J Cryst Growth 46:504–510. https://doi.org/10.1016/0022-0248(79)90038-1
28. Wen X, Wang S, Xie Y, Li XY, Yang S (2005) Low-temperature synthesis of single-crystalline Ag_2S nanowires on silver substrates. J Phys Chem B 109:10100–10106. https://doi.org/10.1021/jp050126o
29. Imanishi Y, Nakaoka T (2018) Room temperature growth of silver telluride nanorods by sputtering deposition. Appl Phys A 124:664. https://doi.org/10.1007/s00339-018-2099-y
30. Zhu J, Pandey R (2019) Silver tellurides: structural, elastic, and optical properties of AgTe and Ag_2Te. J Phys Chem Sol 129:41–45. https://doi.org/10.1016/j.jpcs.2018.12.030
31. Yeh TT, Lin WH, Tzeng WY, Le PH, Luo CW, Milenov TI (2017) The optical properties of Ag_2Te crystals from THz to UV. J Alloys Comp 725:433–440. https://doi.org/10.1016/j.jallcom.2017.07.153
32. Chen C, He X, Gao L, Ma N (2013) Cation exchange-based facile aqueous synthesis of small, stable, and nontoxic near-infrared Ag_2Te/ZnS core/shell quantum dots emitting in the second biological window. ACS Appl Mater Interfaces 5:1149–1155. https://doi.org/10.1021/am302933x
33. Yang M, Gui R, Jin H, Wang Z, Zhang F, Xia J, Bi S, Xia Y (2015) Ag_2Te quantum dots with compact surface coatings of multivalent polymers: ambient one-pot aqueous synthesis and the second near-infrared bioimaging. Colloids Surf B Biointerfaces 126:115–120. https://doi.org/10.1016/j.colsurfb.2014.11.030
34. Xu R, Husmann A, Rosenbaum TF, Saboungi ML, Enderby JE, Littlewood PB (1997) Large magnetoresistance in non-magnetic silver chalcogenides. Nature 390:57–60. https://doi.org/10.1038/36306
35. Schnyders HS (2015) Linear magnetoresistance without linear dispersions: the case of homogeneous silver deficient Ag_2–δTe. Appl Phys Lett 107:042103. https://doi.org/10.1063/1.4927698
36. Premasiri K, Zheng W, Xu B, Ma T, Zhou L, Wu Y, Gao XPA (2019) An electrically driven structural phase transition in single Ag_2Te nanorod devices. Nanoscale 11:6629–6634. https://doi.org/10.1039/c8nr10000d
37. Lee S, In J, Yoo Y et al (2012) Single-crystalline β-Ag_2Te nanorod as a new topological insulator. Nano Lett 12:4194–4199. https://doi.org/10.1021/nl301763r
38. Sulaev A, Zhu W, Teo KL, Wang L (2015) Gate-tuned quantum oscillations of topological surface states in β-Ag_2Te. Sci Rep 5:8062. https://doi.org/10.1038/srep08062
39. Taylor PF, Wood C (1961) Thermoelectric properties of Ag_2Te. J Appl Phys 32:1–3. https://doi.org/10.1063/1.1735932
40. Fujikane M, Kurosaki K, Muta H, Yamanaka S (2005) Electrical properties of a- and b-Ag_2Te. J Alloys Compd 387:297–299. https://doi.org/10.1016/j.jallcom.2004.06.054
41. Pei Y, Heinz NA, Snyder GJ (2011) Alloying to increase the band gap for improving thermoelectric properties of Ag_2Te. J Mat Chem 21:18256. https://doi.org/10.1039/c1jm13888j
42. Chang Y, Guo J, Tang YQ, Zhang YX, Feng J, Ge ZH (2019) Facile synthesis of Ag_2Te nanorods and thermoelectric properties of Ag_2Te polycrystals sintered by spark plasma sintering. CrystEngComm 21:1718–1727. https://doi.org/10.1039/c8ce01863d
43. Jamwal D, Mehta SK (2019) Metal telluride nanomaterials: facile synthesis, properties and applications for third generation devices. Chem Sel 4:1943–1963. https://doi.org/10.1002/slct.201803680
44. Fang H, Wu Y (2014) Telluride nanorod and nanorod heterostructure-based thermoelectric energy harvesting. J Mater Chem A 2:6004–6014. https://doi.org/10.1016/j.ceramint.2017.05.163

45. Park D, Ju H, Kim J (2017) Enhanced thermoelectric power factor and low thermal conductivity in one-dimensional Te/Ag_2Te composites. Ceram Int 43:11156–11162. https://doi.org/10.1016/j.ceramint.2017.05.163
46. Yang H, Bahk JH, Day T, Mohammed AMS, Min B, Snyder GJ, Shakouri A, Wu Y (2014) Composition modulation of Ag_2Te nanorods for tunable electrical and thermal properties. Nano Lett 14:5398–5404. https://doi.org/10.1021/nl502551c
47. Zhou C, Dun C, Ge B et al (2018) Highly robust and flexible n-type thermoelectric film based on Ag_2Te nanoshuttle/polyvinylidene fluoride hybrids. Nanoscale 10:14830–14834. https://doi.org/10.1039/c8nr04883e
48. Zeng X, Yan C, Ren L et al (2018) Silver telluride nanorod assembly for high-performance flexible thermoelectric film and its application in self-powered temperature sensor. Adv Electron Mater 5:1800612. https://doi.org/10.1002/aelm.201800612
49. Seo HJ, Jeong W, Lee S, Moon GD (2018) Ultrathin silver telluride nanorod films and gold nanosheet electrodes for a flexible resistive switching device. Nanoscale 10:5424–5430. https://doi.org/10.1039/c8nr01429a
50. Montaudo G, Puglisi C, Samperi F (1993) Primary thermal degradation mechanisms of PET and PBT. Polym Degrad Stab 42:13–28. https://doi.org/10.1016/0141-3910(93)90021-A
51. Mu L, Wan J, Ma D et al (2005) A room temperature self-sacrificing template route to Ag_2Te fibers. Chem Lett 34:52–53. https://doi.org/10.1246/cl.2005.52
52. Park KR, Kim S, Myung NV, Kang SO, Choa YH (2015) Simple electrochemical synthesis of ultra-long silver telluride nanotubes. RSC Adv 5:29782–29785. https://doi.org/10.1039/c4ra15688a
53. In J et al (2010) In situ TEM observation of heterogeneous phase transition of a constrained single-crystalline Ag_2Te nanowire. Nano Lett 10:4501–4504. https://doi.org/10.1021/nl102350j
54. Lee S, Shin HS, Song JY, Jung M-H (2017) Thermoelectric properties of a single-crystalline Ag_2Te nanorod. J Nanomater 2017:1–5. https://doi.org/10.1155/2017/4308968
55. Bürgermeister A, Sitte W (2001) Chemical diffusion in β-Ag_2Te. Solid State Ion 141–142:331–334. https://doi.org/10.1016/s0167-2738(01)00745-7
56. Okazaki H (1977) Deviation from the Einstein relation in average crystals. II. Self-diffusion of Ag ions in α-Ag_2Te. J Phys Soc Jpn 43:213–221. https://doi.org/10.1143/jpsj.43.213
57. Hamilton MA, Barnes AC, Howells WS, Fischer HE (2001) Ag dynamics in the superionic and liquid phases of Ag_2Se and Ag_2Te by coherent quasi-elastic neutron scattering. J Phys Cond Mat 13:2425–2436. https://doi.org/10.1088/0953-8984/13/11/301
58. Imanishi Y, Hayashi H, Nakaoka T (2018) J Mater Sci 53:12254. https://doi.org/10.1007/s10853-018-2493-z
59. Sáfrán G, Geszti O, Radnóczi G (2003) Transmission electron microscope study of the topotactic reaction of (001), (011) and (111) Ag films and Te. Thin Solid Films 440:261–267
60. Seto Y, Crystallography Software, ReciPro. http://pmsl.planet.sci.kobe-u.ac.jp/~seto/?page_id=19&lang=en/
61. Donadio D, Galli G (2010) Temperature dependence of the thermal conductivity of thin silicon nanowires. Nano Lett 10:847–851. https://doi.org/10.1021/nl903268y
62. Donadio D, Galli G (2009) Atomistic simulations of heat transport in silicon nanowires. Phys Rev Lett 102:195901. https://doi.org/10.1103/PhysRevLett.102.195901
63. Nguyen VD, Pham N (1968) Transport properties of silver telluride in the solid and liquid states. Phys Stat Sol 30:557–567. https://doi.org/10.1002/pssb.19680300217
64. Zhan T, Xu Y, Goto M, Tanaka Y, Kato R, Sasaki M, Kagawa Y (2014) Thermal conductivity of sputtered amorphous Ge films. AIP Adv 4:027126. https://doi.org/10.1063/1.4867122
65. Markussen T (2012) Surface disordered Ge–Si core-shell nanowires as efficient thermoelectric materials. Nano Lett 12:4698–4704. https://doi.org/10.1021/nl302061f